International Journal of
Plasma Environmental Science and Technology

Regular Paper DOI: 10.34343/ijpest.2025.19.e01009

Reduction of carbon dioxide particles to carbon monoxide by nonthermal plasma

Haruhiko Yamasaki*, Takafumi Kida, Tomoyuki Kuroki, Masaaki Okubo

Department of Mechanical Engineering, Osaka Metropolitan University, Japan

* Corresponding author: hyamasaki@omu.ac.jp (Haruhiko Yamasaki)

Received: 30 December 2024
Revised: 19 February 2025
Accepted: 12 March 2025
Published online: 28 March 2025

Abstract

Nonthermal plasma reduces carbon dioxide to carbon monoxide, which can be converted into fuels and organic compounds, and is used as a raw material for gas synthesis. However, the energy efficiency is currently too low for practical use, and innovative ideas are required. This study proposes a CO_2 fuel conversion technology using solid CO_2 in a nonthermal plasma reactor. The advantages of using solid CO_2 are the suppression of the CO re-oxidation reaction at low temperatures and the improvement in energy efficiency at high CO_2 concentrations. In the experiment, the plasma reduction of gaseous and solid CO_2 is performed using a dielectric barrier discharge plasma reactor, and the conversion and energy efficiencies are compared. The concentration of generated CO is found to be dependent on the concentration of CO_2. When nonthermal plasma is applied to solid CO_2, Joule heating causes CO_2 sublimation, which reduces gaseous CO_2 to CO. The solid CO_2 in the plasma reactor increases the impedance and decreases the discharge power. The introduction of solid CO_2 upstream of the reactor increases the discharge power and improves the CO conversion efficiency. At a specific energy of 1.8 eV/molecule, the reduction of solid CO_2 increases the conversion efficiency from 1.4% to 1.8% and the energy efficiency from 2.3% to 2.7%, compared to the reduction of gaseous CO_2.

Keywords: Nonthermal plasma, carbon dioxide, carbon monoxide, solid-phase of CO_2, dielectric barrier discharge.

1. Introduction

The concentration of carbon dioxide (CO_2) in the atmosphere has increased significantly due to the burning of fossil fuels and deforestation. CO_2 is a greenhouse gas that absorbs heat radiated from the Earth's surface to outer space and radiates it back to the surface. As the concentration of CO_2 in the atmosphere increases, global warming progresses, causing serious damage to the global environment, such as increasing sea levels, unusual weather, and ecosystem destruction. Therefore, technologies for capturing and treating CO_2 have become increasingly important.

Carbon capture and storage (CCS) is a promising technology for reducing emissions and is projected to account for 14% of cumulative CO_2 emission reductions by 2050 [1]. CCS involves capturing and separating CO_2 from fossil fuel-fired power plants, transporting it to a designated storage site, and injecting it into a suitable carbon-bearing layer deep beneath the ocean. In the separation portion, CO_2 can be isolated using cryogenic separation, membrane separation, or sorbents such as chemical absorption and solid adsorption. Typical sorbents include molecular sieves, zeolites, calcium oxides, hydrotalcites, and lithium zirconate [2]. These methods achieve approximately 100% CO_2 concentration. However, the current adsorption technologies are expensive [3]. Therefore, there is a need for CO_2 treatment technologies that are both cost-effective and highly efficient to ensure sustainable CO_2 emission reduction.

By contrast, CO_2 conversion technology to carbon monoxide (CO) or C1 materials using metal catalysts or photocatalysts has also been proposed [4–9]. CO is converted to syngas when mixed with hydrogen (H_2) and has been studied for use as a fuel in gas-turbine engines [10, 11]. In addition to catalytic technology, nonthermal plasma (NTP) is widely used for converting CO_2 to CO at atmospheric pressure and temperature [12–24]. CO_2 reduction is achieved by applying an NTP characterized by fast electrons and atmospheric discharge. In NTP-based technology, CO_2 is mainly reduced to CO via a plasma chemical reaction [25], as shown in (1)

$$CO_2 \rightarrow CO + O_2/2, \qquad \Delta H = 2.9 \text{ eV/molecule}, \tag{1}$$

where ΔH is the enthalpy of the reaction. In addition, the following reactions (2) and (3) are the major reactions of CO_2 reduction in the plasma reactor. However, these two reactions are considered negligible in this study due to the low power density of plasma generation [26].

$$CO_2 + M \rightarrow CO + O + M, \tag{2}$$

$$CO_2 + O \rightarrow CO + O_2, \tag{3}$$

where M is third body in the reaction process. One challenge of this technology is its energy efficiency. Ideally, this can be reduced to 2.9 eV/molecule; currently, more than twice the amount of energy must be invested. Identifying the source of CO_2 is challenging. For example, flue gas from a thermal power plant has a CO_2 concentration of approximately 10%, and more energy is required to increase this concentration from 10% to 100% to improve energy efficiency. This challenge is more significant for CO_2 in air at 400–500 ppm. Our research group proposed a technology that simultaneously conducts CO_2 adsorption/concentration and reduction with an NTP by combining an adsorbent with NTP [27–29]. Results of CO_2 concentration and reduction in simulated combustion exhaust gas and air show relatively good results of CO_2 conversion and energy efficiency of 21% and 13%, respectively; however, further improvement of energy efficiency is required for practical use.

To improve the energy efficiency, Lu *et al*. [30] cooled plasma reactors. By cooling the plasma reactor temperature from 120 °C to 40 °C by water cooling, a 6% increase in CO conversion efficiency and 2% improvement in energy efficiency have been reported. Decreasing the temperature of the reaction region of the reactor suppresses the recombination reactions to CO_2 and improves the effective utilization rate of the input energy in the reaction system. Berthelot and Bogaerts [26] modelled CO_2 reduction using microwave plasma and the effects of pressure and temperature on energy efficiency.

Based on this background, this study performs NTP reduction on solid-phase CO_2 particles called dry ice particles, considering that NTP treatment of CO_2 at lower temperatures and higher densities may improve energy efficiency. CO_2 separated and recovered from flue gas using adsorbents or membrane separation is generally transported and stored in a gaseous state for short-distance transportation or immediate use, whereas it is transported and stored in liquid and solid states for long-distance transportation or storage purposes. CO_2 in the liquid state can be easily converted into solid CO_2 through adiabatic expansion. Therefore, this study focuses on solid CO_2, which has a higher density than the gaseous state, and aims to verify the effectiveness of a CO_2 reduction system using solid CO_2 and evaluate the energy efficiency of the NTP reduction technology for solid CO_2.

2. Experimental

Fig. 1 shows a schematic of the experimental setup for solid CO_2 reduction using a dielectric barrier discharge plasma reactor. The experimental apparatus comprises an N_2 cylinder, mass flow meter, plasma reactor, pulsed high-voltage power supply, oscilloscope, data logger, and gas analyzer. A mass-flow controller (SFC-281E, Hitachi Metals, Ltd., Japan) is used to adjust the flow rate of the N_2 cylinder (purity = 99.995%). N_2 gas flows from the top of the plasma reactor filled with solid CO_2 particles, and the reactor is energized with a high voltage to generate NTP and reduce CO_2 to CO. The treated gas flows from the bottom of the reactor, and the concentrations are measured using a CO_2, CO, O_2, NO, and NO_x analyzer (PG350, Horiba, Ltd., Japan; CO_2 < 20%, CO < 5000 ppm, O_2 < 25%, NO < 2500 ppm, NO_x < 2500 ppm). Fig. 2 shows a detailed schematic of the plasma reactor. The plasma reactor comprises a discharge wire, quartz tube, grounding electrode, and an insulator. The quartz tube is a cylindrical tube with an inner diameter of 20 mm, outer diameter of 25 mm, a length of 646 mm, and a 0.05 mm thick ground electrode in a 260 mm longitudinal section (discharge area). The discharge wire is made of stainless steel with a diameter of 2.0 mm and is placed at the radial center of the quartz tube. An insulated gate bipolar transistor (IGBT) pulsed high-voltage power supply (PPCP Pulsar SHC-30/1000, Masuda Research Inc., Japan) is used as the plasma power supply, and a high voltage is applied to the discharge wire to generate NTP between the wire and ground electrode. The voltage applied to the reactor and discharge current are measured with an oscilloscope (DLM2054, Yokogawa Electric Co., Japan)

using a voltage probe (P6015A, conversion factor = 1 kV/V, Tektronix Inc.) and a current probe (P6021, conversion factor = 10 A/V, Tektronix Inc.). The discharge mode is a pulsed dielectric barrier discharge (DBD). Solid CO_2 is generated by the adiabatic expansion of CO_2 from a liquid CO_2 cylinder, and the mass is measured before filling part of the reactor. To generate solid CO_2, silica gel is placed in the generation vessel to prevent coagulation and binding with moisture in the air, and the vessel is vacuumed after CO_2 purging to sufficiently remove moisture before generation. Fig. 3 shows a photograph of the solid CO_2 particles generated. The particles are irregularly shaped and range in diameter from 0.5 to 5.0 mm with an average particle size of approximately 1 mm.

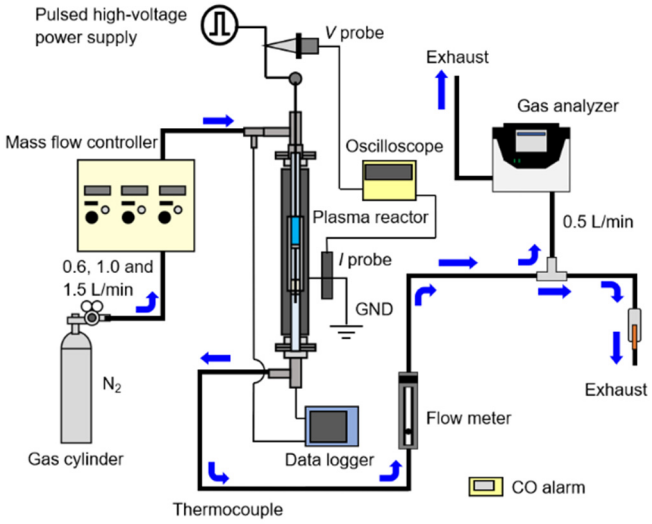

Fig. 1. Schematic of experimental setup.

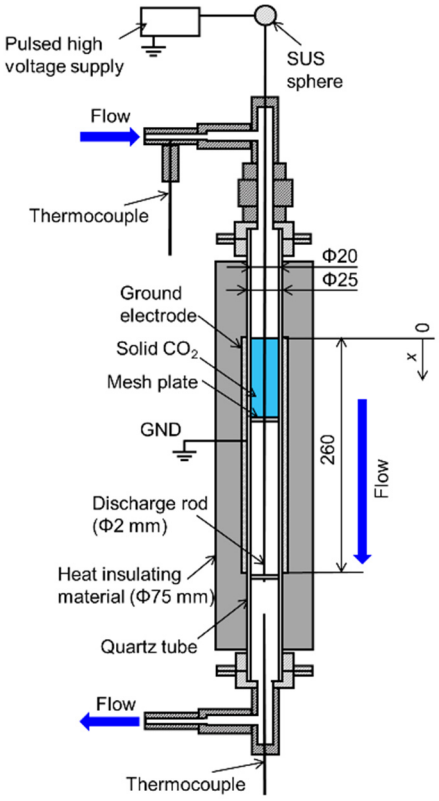

Fig. 2. Plasma reactor.

The experimental conditions are as follows: solid CO_2 is filled in the range of x = −100–0, 0–50, 0–100, 0–150 mm, N_2 flow rate 0.6, 1.0, and 1.5 L min^{-1}, voltage 20–26 kV, voltage frequency 210, 520, and 840 Hz. Here, x = 0 indicates the upper end of the discharge region of the reactor, and minus indicates the upstream end of the reactor. The experiment is conducted until the solid CO_2 has completely sublimated and the gas concentration has reached a steady state to prevent excessive temperature increases in the reactor. This study includes a gaseous CO_2 reduction experiment for comparison. Gaseous CO_2 reduction experiments are performed using CO_2 and N_2 cylinders with a mixture of CO_2 = 20% and N_2 = 80% by adjusting the flow rate using a mass flow meter, changing the applied pulse frequency to 210, 520, and 840 Hz, and discharging it for 10 min. The CO conversion efficiency α and energy efficiency η are used to evaluate the experiment. α represents the fraction of CO_2 molecules that are reduced to CO and is determined by Equation (4) from CO_2 and CO concentration, while energy efficiency is determined by Equation (5).

$$\alpha = \mathrm{CO} / (\mathrm{CO}+\mathrm{CO_2}) \times 100 \tag{4}$$

$$\eta = \alpha \times \frac{\Delta H}{E_v} \tag{5}$$

Here, E_v is the specific energy of the plasma obtained from the discharge power P (W) and gas flow rate Q (L min^{-1}) using the following equation:

$$E_{\mathrm{V}} = \left(\frac{P}{1.602\times10^{-19}} \right) / \left(\frac{CO_2 \times Q}{60} \times 22.4 \times 6.02 \times 10^{23} \times \frac{273.15}{T} \right) \tag{6}$$

where T (K) is room temperature.

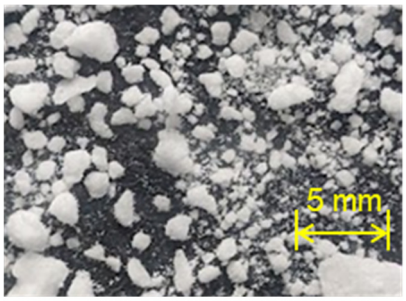

Fig. 3. Photograph of solid CO_2 particles.

3. Results and discussion

3.1 Effect of N_2 flow rate on CO and CO_2 concentration

Figs. 4 (a)–(c) show the experimental results of the time-dependent CO_2 and CO concentrations for a solid CO_2 filling range of x = 0–100 mm, pulse frequency of 210 Hz, and N_2 flow rates of (a) 0.6 L min^{-1}, (b) 1.0, and (c) 1.5 L min^{-1}. As shown in Fig. 4 (a), the initial concentration of CO_2 is 26%, which is caused by the sublimation of solid-phase CO_2 to gaseous CO_2 owing to the forced thermal convection caused by the N_2 flow and Joule heating caused by the discharge. CO_2 decreases with time, and no CO_2 is detected after 15 min. CO is generated immediately after the start of the discharge, increasing to a maximum of 3147 ppm at 7 min and decreasing as CO_2 decreases. The CO_2 flow rate, calculated from the N_2 flow rate and CO and CO_2 concentrations, gradually decreases from 0.23 L min^{-1} at 1 min to 0.21 L min^{-1} at 7 min. As shown in Fig. 4 (b), the initial concentration of CO_2 is 24% and CO_2 decreases with time, and no CO_2 is detected after 15 min. CO is generated immediately after the start of the discharge, increasing to a maximum of 1791 ppm at 7 min,

and decreasing as CO_2 decreases. The CO_2 flow rate gradually decreases from 0.30 L min^{-1} at 1 min to 0.29 L min^{-1} at 7 min. As shown in Fig. 4 (c), the initial concentration of CO_2 is 23%; CO_2 decreases with time, and no CO_2 is detected after 16 min. CO is generated immediately after the start of the discharge and increases to a maximum of 1273 ppm at 3 min, gradually decreasing by 100 ppm at 10 min, and then decreasing to zero after 10 min. The CO_2 flow rate gradually decreases from 0.46 L min^{-1} at 1 min to 0.39 L min^{-1} at 3 min and 0.31 L min^{-1} at 10 min. The figures show that the CO concentration decreases as the N_2 flow rate increases. This is caused by a decrease in residence time. The residence times calculated from the mixed flow rate and the discharge region (0.08 L) when the CO concentration is at its maximum are 6.0, 3.8, and 2.6 s for N_2 flow rates of 0.6, 1.0, and 1.5 L min^{-1}, respectively. This indicates that the CO concentration depends on the residence time. The time required for all solid CO_2 to sublimate is approximately 15 min in all cases, indicating that Joule heating, rather than forced thermal convection, is dominant for solid CO_2 sublimation.

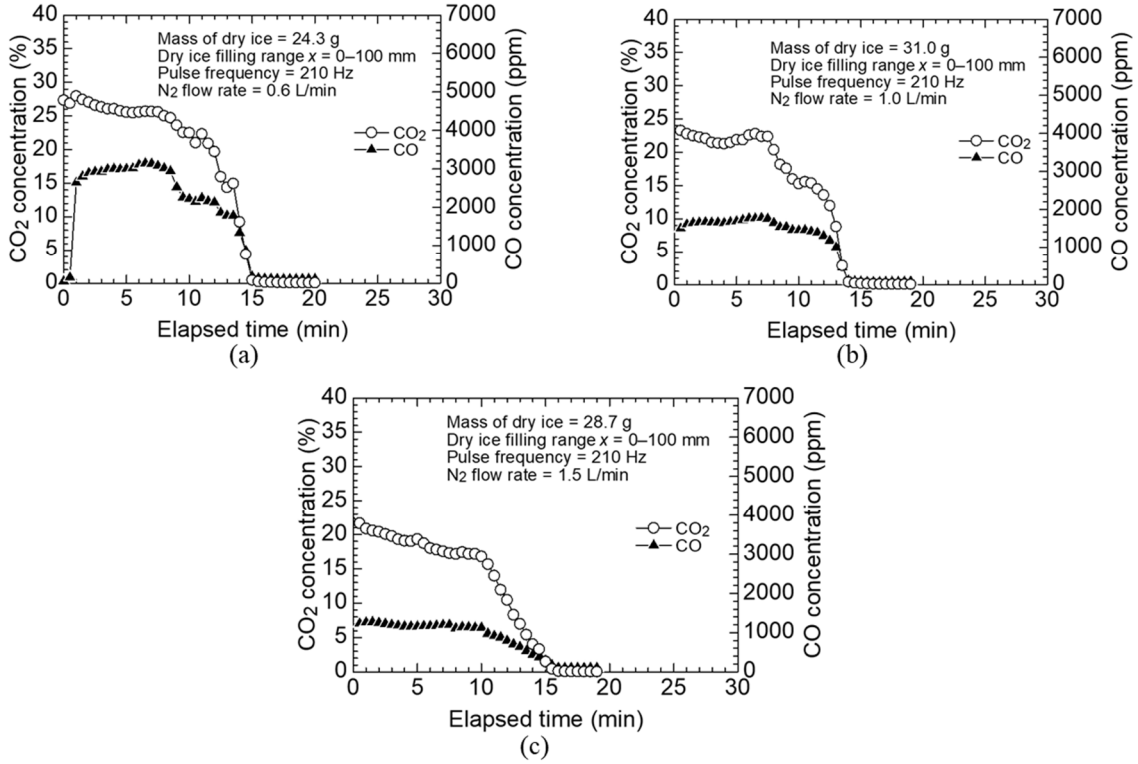

Fig. 4. Time-dependent CO_2 and CO concentrations at f = 210 Hz and x = 0−100 mm (a) N_2 = 1.0 L min^{-1}, (b) N_2 = 1.0 L min^{-1}, (c) N_2 = 1.0 L min^{-1}.

Fig. 5 (a)–(c) show the discharge power during the experiment for a solid CO_2 filling range of x = 0–100 mm, a pulse frequency of 210 Hz, and N_2 flow rates of (a) 0.6 L min^{-1}, (b) 1.0, and (c) 1.5 L min^{-1}. As shown in Fig. 5 (a), at the beginning of the discharge, the discharge power is 14 W, which is lower than the 35 W of N_2 plasma without solid CO_2 particle, owing to the large amount of solid CO_2 and the high impedance of solid CO_2. As the elapsed time increases, the solid CO_2 sublimates owing to Joule heating, causing a void to form around the discharge wire. The voids cause a decrease in the impedance, which increases the discharge power, resulting in an increase in the CO concentration. After 15 min, the discharge power reaches 35 W, which is the same as that of the N_2 plasma. As shown in Fig. 5 (a)–(c), as the N_2 flow rate is increased, there is no significant change in the CO_2 sublimation rate; therefore, there is no significant change in the discharging power.

Fig. 6 (a) and (b) show the waveforms of the voltage V, current I, and instantaneous power at a solid CO_2 filling range of x = 0–100 mm, pulse frequency of 210 Hz, N_2 flow rate of 1.0 L min^{-1}, and elapsed times of (a) 1 min and (b) 7 min. The discharge mode is pulsed DBD. The discharge power averaged over time, as shown in Fig. 4, is determined by integrating the instantaneous power of the positive region as an effective power throughout a single cycle and then multiplying it by the pulse frequency f and conversion factors of the current and voltage probes. As shown in Fig. 6 (a), discharge occurs even in the early stages because it occurs in areas where dry ice particles are not present in the discharge region. As the elapsed time and discharge

power increase, the width of the current increases. This indicates that as the discharge region increases, the energy supplied to the molecules by the discharge increases, and the CO concentration increases.

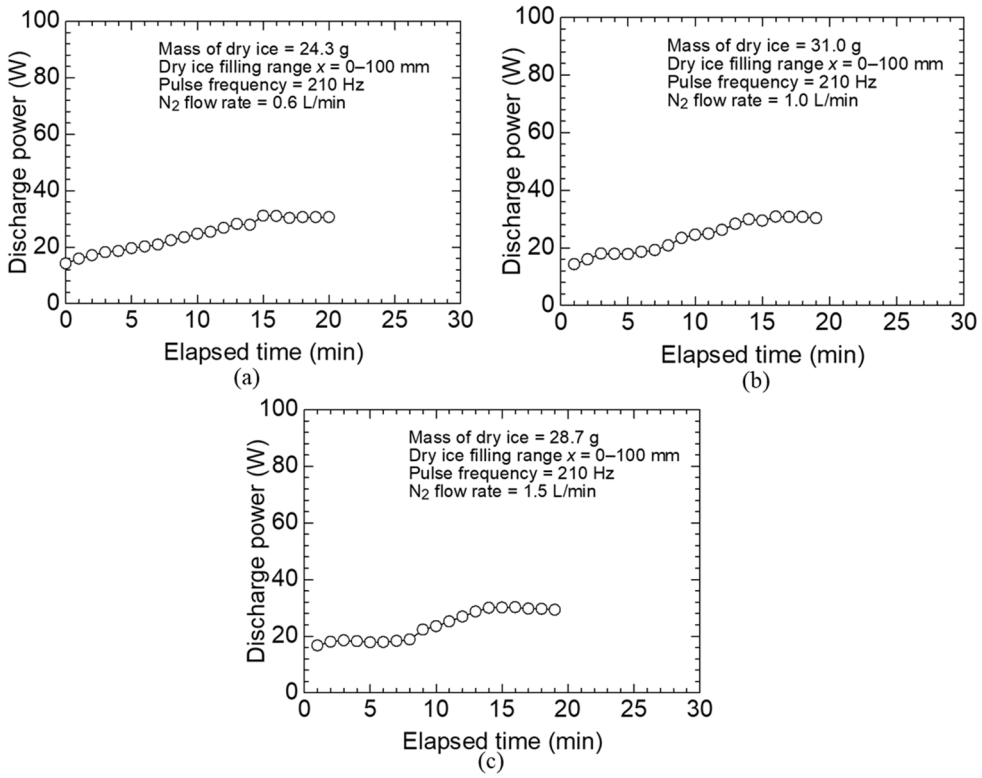

Fig. 5. Time-dependent discharge power at f = 210 Hz, x = 0−100 mm, and (a) N_2 = 1.0 L min^{-1}, (b) N_2 = 1.0 L min^{-1}, (c) N_2 = 1.0 L min^{-1}.

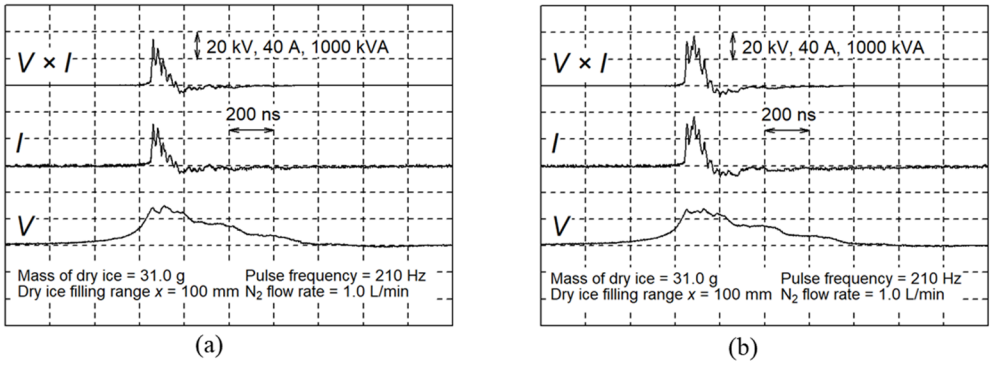

Fig. 6. Waveforms of the voltage V, current I, and instantaneous power at a solid CO_2 filling range of x = 0–100 mm, a pulse frequency of 210 Hz, N_2 flow rate of 1.0 L min^{-1}, and elapsed time of (a) 1 min and (b) 7 min.

3.2 Effect of CO_2 particle filling volume on CO and CO_2 concentration

Figs. 7 (a) and (b) show the experimental results of the time-dependent CO_2 and CO concentrations for a pulse frequency of 210 Hz, an N_2 flow rate of 1.0 L min^{-1}, and solid CO_2 filling ranges of (a) x = 0–50 mm and (b) x = 0–150 mm. As shown in Fig. 7 (a), the initial concentration of CO_2 is 25%, which decreases until a treatment time of 10 min, after which no CO_2 is detected. CO is generated immediately after the start of the discharge, reaching a maximum of 2500 ppm and decreasing as CO_2 decreases. The maximum CO_2 flow rate is 0.37 L min^{-1} at 1 min. As shown in Fig. 7 (b), the initial concentration of CO_2 is 26%, which decreases until the treatment time of 21 min, after which no CO_2 is detected. CO is generated immediately after the start of the discharge, gradually increases, reaches a maximum of 1000 ppm at 15 min, and then decreases. The maximum CO_2 flow rate is 0.36 L min^{-1} at 1 min and the average CO_2 flow rate is 0.34 L min^{-1} for 0–10 min.

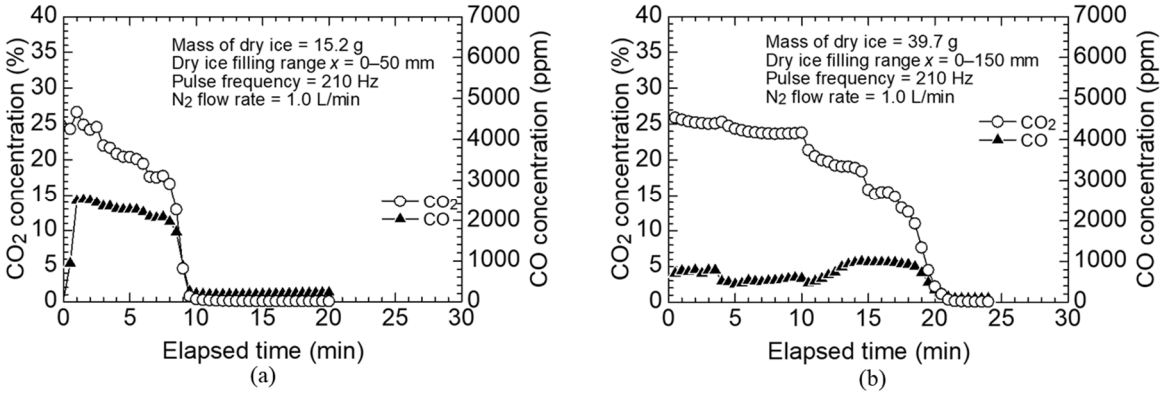

Fig. 7. Time-dependent CO_2 and CO concentrations at f = 210 Hz, N_2 = 1.0 L min^{-1}, and (a) x = 0–50 mm and (b) x = 0–150 mm.

Figs. 8 (a) and (b) show the discharge power for a pulse frequency of 210 Hz, an N_2 flow rate of 1.0 L min^{-1}, and solid CO_2 filling ranges of (a) x = 0–50 mm and (b) x = 0–150 mm. As shown in Fig. 8 (a), the initial discharge power is 20 W, increasing to 12 min and remaining steady at 37 W. Visual observation of the discharge region above the reactor confirms that the plasma produced strong light around the discharge wire and near the inner wall of the quartz tube, whereas weak light is observed between the CO_2 particles. As shown in Fig. 8 (b), the initial discharge power is 8 W. The discharge power does not increase until 10 min, and then increases and becomes steady at 31 W for 21 min. This is because the amount of CO_2 filling is high, and it takes time for the CO_2 particles to sublimate near the inner wall of the quartz tube. As shown in Fig. 7 (b), CO_2 decreases from 10 to 15 min, but the increase in CO concentration is caused by an increase in the discharge power owing to the creation of a sufficient gas-phase gap on the inner wall of the quartz tube to promote discharge. However, the decrease in CO concentration compared to that shown in Fig. 7 (a) is caused by the greater impact of the decrease in CO_2 concentration than the increase in CO concentration that can be expected from the increase in discharge power.

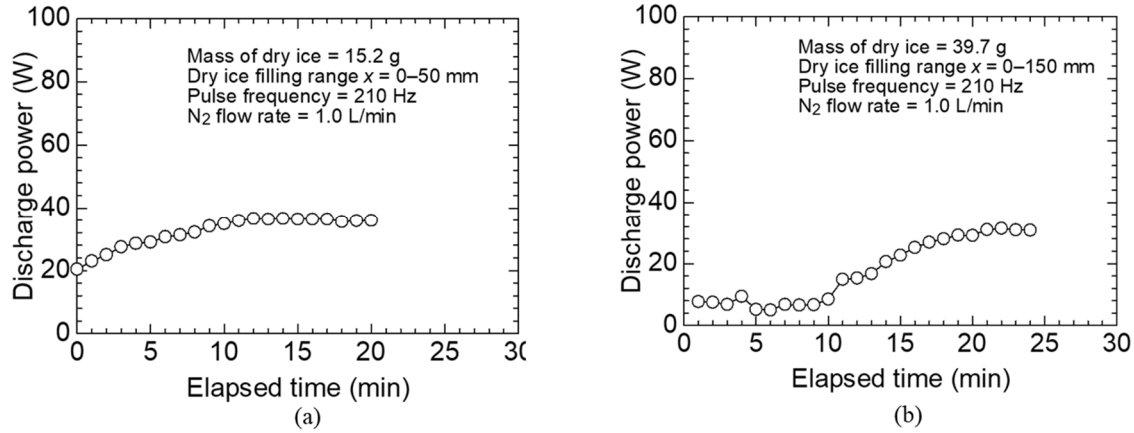

Fig. 8. Time-dependent discharge power at f = 210 Hz, N_2 = 1.0 L min^{-1}, and (a) x = 0–50 mm and (b) x = 0–150 mm.

3.3 Effect of CO_2 particle filling upstream of the reactor on CO and CO_2 concentration

The results shown in Figs. 4 and 7 reveal that expanding the discharge area and increasing the CO_2 concentration leads to an increase in the CO concentration. To establish a synergistic relationship with the cooling effect of solid CO_2 particles, experiments in which solid CO_2 particles are filled upstream of the discharge area are conducted. Figs. 9 (a)–(c) show the experimental results of time-dependent CO_2 and CO concentrations for a solid CO_2 filling range of x = −100–0 mm upstream of the reactor, an N_2 flow rate of 1.0 L min^{-1}, and (a) pulse frequency of 210 Hz, (b) 520 Hz, and (c) 840 Hz. As shown in Fig. 9 (a), the initial concentration of CO_2 is 24%, which decreases until a treatment time of 15 min, after which no CO_2 is detected. CO is generated immediately after the start of the discharge, reaching a maximum of 2780 ppm and decreasing

as CO_2 decreases. The residence time at the maximum CO concentration is 0.06 s. From Fig. 9 (b), the initial concentration of CO_2 is 27% and decreases until the treatment time of 23 min, after which no CO_2 is detected. CO is generated immediately after the start of the discharge, reaching a maximum of 4506 ppm and decreases as CO_2 decreases. As shown in Fig. 9 (c), the initial concentration of CO_2 is 27% and decreases after 20 min. In this case, the measurement was stopped after 20 min because the reactor temperature reached the thermal resistance of the insulator. CO is generated immediately after the start of the discharge, reaching a maximum of 4716 ppm and decreasing as CO_2 decreases.

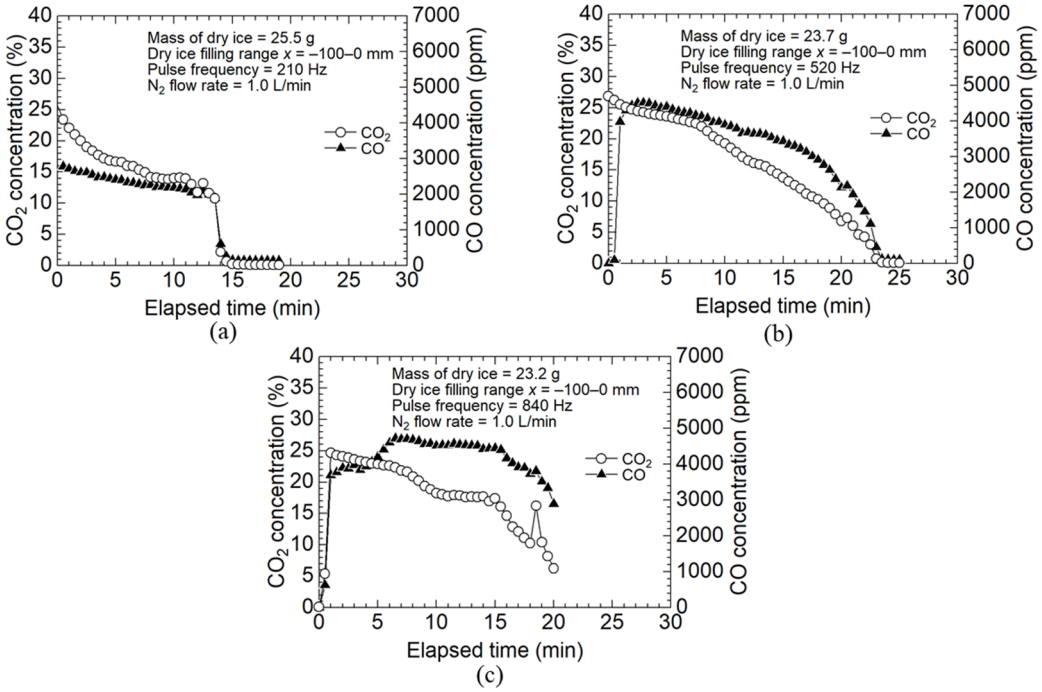

Fig. 9. Time-dependent CO_2 and CO concentrations at $x = -100–0$ mm, $N_2 = 1.0$ L min^{-1}, and (a) $f = 210$ Hz, (b) $f = 520$ Hz, and (c) $f = 840$ Hz.

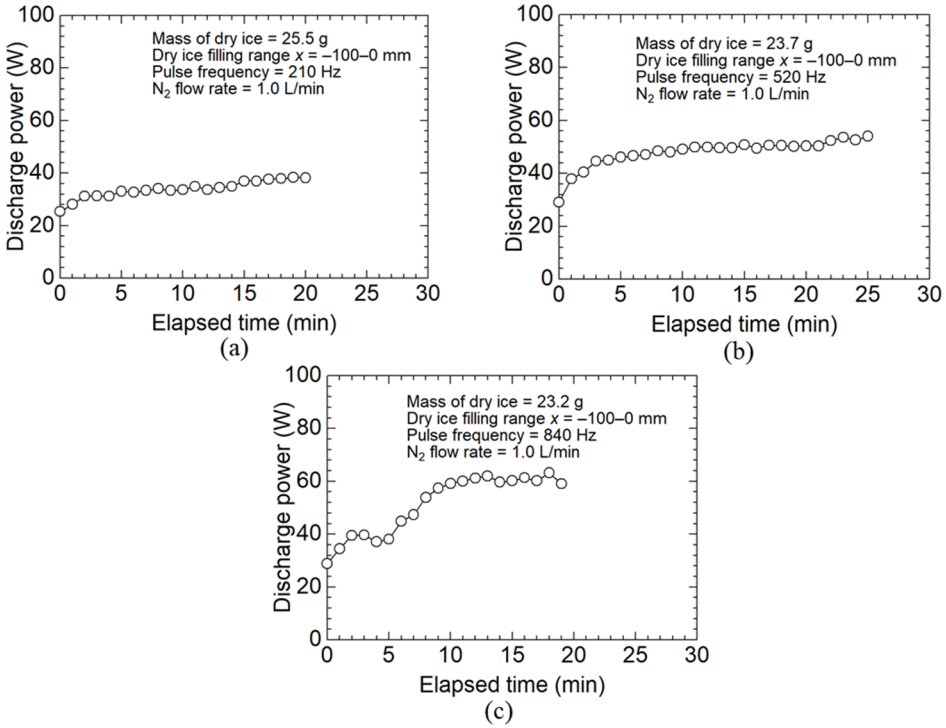

Fig. 10. Time-dependent discharge power at $x = -100–0$ mm, $N_2 = 1.0$ L min^{-1}, and (a) $f = 210$ Hz, (b) $f = 520$ Hz, and (c) $f = 840$ Hz.

Figs. 10 (a)–(c) show the discharge power during the experiment for a solid CO_2 filling range of $x = -100$–0 mm upstream of the reactor, an N_2 flow rate of 1.0 L min^{-1}, and (a) pulse frequency of 210 Hz, (b) 520 Hz, and (c) 840 Hz. In Fig. 10 (a), the initial discharge power is 25 W, which increases up to 15 min and is steady at 38 W. The discharge power increases over time even without solid CO_2 particles in the discharge region, because the solid CO_2 particles lower the temperature of the gas in the discharge region and ground electrode, resulting in a decrease in electrical conductivity and increase in impedance. As the elapsed time increases, the temperatures of the quartz tube and ground electrode increase owing to the heat from the discharge, and the impedance decreases, resulting in an increase in the discharge power. In Fig. 10 (b), the initial discharge power is 29 W, which then increases gradually and saturates at 51 W after 11 min. In Fig. 10 (c), the initial discharge power is 28 W, which then increases gradually and saturates at 61 W at 11 min. As the pulse frequency increases to 210, 520, and 840 Hz and the discharge voltage decreases to 26, 23, and 22 kV, the discharge power increases, but not proportionally. When solid CO_2 is filled upstream of the reactor, the CO concentration increases due to the higher discharge power from the beginning and the increased residence time of gaseous CO_2.The discharge power and CO concentration increase with increasing pulse frequency.

3.4 CO conversion and energy efficiencies

Fig. 11 shows the conversion efficiency α and energy efficiency η versus specific energy E_v for the experiment using solid CO_2 and the reduction of gaseous CO_2 using cylinder gas. Because CO_2 and CO concentrations are unsteady in elapsed time due to CO_2 sublimation, α and η here denote the η that reaches a maximum during the treatment time and α at that time. As E_v increases, α increases because more energy is given to the CO_2 molecules. η is a function of α and E_v as shown in Eq. (5), and in this study range, η decreases as E_v increases because E_v varies more than α. The results of the experiment using cylinder gas at a CO_2 concentration of 20%, which is equivalent to the CO_2 produced during solid CO_2 reduction, show a high E_v owing to the absence of solid CO_2, which decreases the impedance in the reactor and increases the discharge power. Comparing the case with the same E_v, solid CO_2 filled upstream of the discharge area of the reactor ($x = -100$–0 mm), N_2 flow rate 1.0 L min^{-1}, and discharge frequency 520 Hz with cylinder gas and discharge frequency 210 Hz, the energy efficiency η is 2.7% and 2.3%, respectively, and the conversion efficiencies α are 1.8% and 1.4%, respectively. The introduction of solid CO_2 upstream of the reactor increases α and η by 0.4% each. This is because the solid CO_2 cools the reactor and promotes reduction. However, when the discharge area is filled with solid CO_2, the results show a similar trend to those obtained with cylinder gas. This is because of the large impedance of solid CO_2, which results in a lower discharge power, and it is difficult to achieve the effect of promoting reduction at low temperatures. These results show that filling solid CO_2 upstream of the discharge region ($x = -100$–0 mm), decreasing the N_2 flow rate, increasing the discharge frequency, and increasing E_v increases α and η.

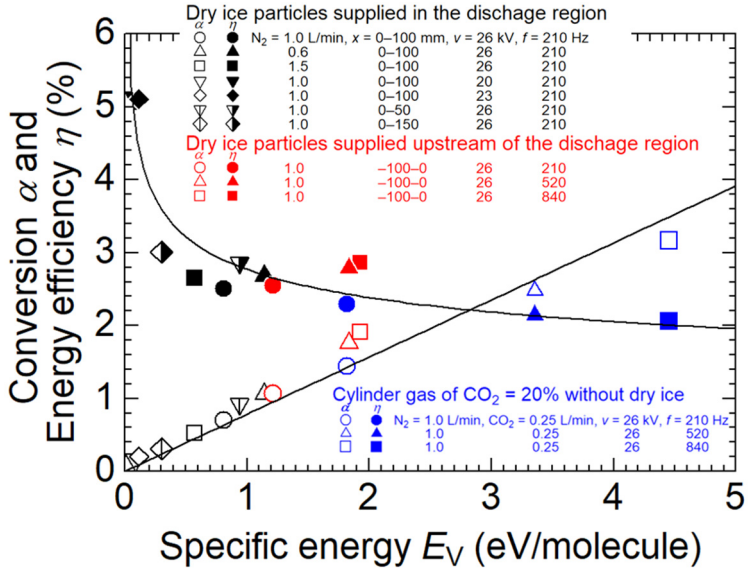

Fig. 11. Relationships between specific energy (E_v), conversion efficiency (α), and energy efficiency (η).

4. Conclusion

To improve the energy efficiency of CO_2 reduction, solid-phase CO_2 reduction using a DBD reactor was performed by varying the gas flow rate, applied voltage frequency, and dry ice introduction point. The main results are summarized as follows:

1. Joule heat, rather than forced thermal convection, is dominant the solid CO_2 sublimation, and CO is generated immediately after discharge. When the N_2 flow rate is 0.6 L min^{-1} at a pulse frequency of 210 Hz and the solid CO_2 filling range of x = 0–100 mm, CO_2 and CO reach 26% and 3147 ppm, respectively. As the N_2 flow rate decreases, the CO concentration increases because the residence time in the reactor increases.
2. When the N_2 flow rate is 1.0 L min^{-1} at a pulse frequency of 210 Hz and the solid CO_2 filling range of x = 0–50 mm, CO_2 and CO reach 25% and 2500 ppm, respectively, and the decrease in the solid CO_2 filling volume decreases the impedance and increased the discharge power. Therefore, even when the solid CO_2 filling volume is increased, the amount of CO is lower because of the decrease in discharge power.
3. When dry ice is filled upstream of the discharge region, the CO concentration increases due to higher discharge power and increased residence time of gaseous CO_2, achieving a maximum energy efficiency η of 2.8% and conversion efficiency α of 1.9%.
4. Comparing solid CO_2 filled upstream of the discharge region of the reactor (x = −100–0 mm) with cylinder gas at the same E_v (= 1.8 eV/molecule), η was 2.7% and 2.3% and α was 1.8% and 1.4%, an increase of 0.4%, respectively. Both η and α increase due to the cooling of the reactor by the solid CO_2 particles.

Acknowledgment

The authors thank Mr. H. Wakimoto and Mr. G. Kato, graduate students at Osaka Prefecture University and Osaka Metropolitan University, respectively, for conducting the experiments. This study was partially supported by JSPS KAKENHI (Grant umber JP24K15340).

References

[1] International Energy Agency edition, Energy Technology Perspective 2017, IEA Publications, France, 2017.
[2] Leung D. Y., Caramanna G., and Maroto-Valer M. M., An overview of current status of carbon dioxide capture and storage technologies, *Renew. Sust. Enegy. Rev*., Vol. 39, pp. 426–443, 2014.
[3] T. Inui (ed.), CO_2 Fixed/Separation Technology (in Japanese), Tokyo: CMC Publishing, pp. 69–123, 2006.
[4] Yusuf N., Almomani F., and Qiblawey H., Catalytic CO_2 conversion to C1 value-added products: Review on latest catalytic and process developments, *Fuel*, Vol. 345, 128178, 2023.
[5] Habisreutinger S. N., Schmidt-Mende L., and Stolarczyk J. K., Photocatalytic reduction of CO_2 on TiO_2 and other semiconductors, *Angew. Chem. Int. Ed*., Vol. 52, pp. 7372–7408, 2013.
[6] Fu Z., Yang Q., Liu Z., Chen F., Yao F., Xie T., Zhong Y., Wang D., Li J., Li X., and Zeng G., Photocatalytic conversion of carbon dioxide: From products to design the catalysts, *J CO_2 Util*., Vol. 34, pp. 63–73, 2019.
[7] Alli, Y.A., Oladoye, P.O., Onawole, A.T., Hazleen A., Sheriff A., Ogunbiyi, O.D., and Philippot, K., Photocatalysts for CO_2 reduction and computational insights, *Fuel*, Vol. 344, 128101, 2023.
[8] Guo R, Xia C., Bi Z., Zhang Z., and Pan W, Recent progress of photothermal effect on photocatalytic reduction of CO_2, *Fuel Process. Technol*., Vol. 241, 107617, 2023.
[9] Wei C., Ding H., Zhang, Z., Lin F. Xu Y., and Pan W, Research progress of bimetallic catalysts for CO_2 hydrogenation to methane, *Int. J. Hydrogen Energy*, Vol. 58, pp. 872–891, 2024.
[10] Pradhan A., Baredar P., and Kumar A., Syngas as an alternative fuel used in internal combustion engines: a review, *J. Pure Appl. Sci. Technol.* Vol. 5, pp. 51–66, 2015.
[11] Wright I. G. and Gibbons T. B., Recent developments in gas turbine materials and technology and their implications for syngas firing, *Int. J. Hydrog. Energy*, Vol. 32, pp. 3610–3621, 2017.
[12] Snoeckx R. and Bogaerts A., Plasma technology - a novel solution for CO_2 conversion?, *Chem. Soc. Rev*., Vol. 46, pp. 5805–5863, 2017.
[13] Bogaerts A. and Neyts E.C., Plasma technology: An emerging technology for energy storage, *ACS Energy Lett.,* Vol. 3, pp. 1013–1027, 2018.
[14] Luo Y., Yue X., Zhang H., Liu X., and Wu Z., Recent advances in energy efficiency optimization methods for plasma CO_2 conversion, *Sci. Total Environ*., Vol. 906, 167486, 2024.

[15] Li S., Felice G.D., Eichkorn S. Shao T., and Gallucci F., A review on plasma-based CO_2 utilization: process considerations in the development of sustainable chemical production, *Plasma Sci. Technol*., Vol. 26, 094001, 2024.
[16] Vertongen R., Felice G.D., Bogaard H., Gallucci F., Bogaerts A., and Li S., Sorption-enhanced dry reforming of methane in a DBD plasma reactor for single-stage carbon capture and utilization, *ACS Sustainable Chem. Eng*., Vol. 12, pp. 10841−10853, 2024.
[17] Ong, M.Y., Nomanbhay, S., Kusumo, F., and Show, P.L., Application of microwave plasma technology to convert carbon dioxide (CO_2) into high value products: A review, *J. Clean Prod.*, Vol. 336, 130447, 2022.
[18] Rao, M.U., Vidyasagar, D., Rangappa, H.S., Subrahmanyam, C., Recent advances on CO_2 conversion into value added fuels by non-thermal plasma, *Catal. Today*, Vol. 41, 114887, 2024.
[19] Kiefer, C.K., Antunes, R., Hecimovic, A., Meindl, A., and Fantz, U., CO_2 dissociation using a lab-scale microwave plasma torch: An experimental study in view of industrial application, *Chem. Eng. J*., Vol. 481, 148326, 2024.
[20] Attri, P., Okumura, T., Takeuchi, N., Kamataki K., Koga, K., and Shiratani, M., Influence of humidity on the plasma-assisted CO_2 conversion, *Plasma Process. Polym*., Vol. 481, 148326, 2024.
[21] Mahdikia, H., Brüser, V., Schiorlin, M., Brandenburg, R., CO_2 Dissociation in Barrier Corona Discharges: Effect of Elevated Pressures in CO_2/Ar Mixtures, *Plasma Chem. Plasma Process*., Vol. 43, pp. 2035–2063, 2023.
[22] Emeraldi, P., Imai, T., Hayakawa, Y., Kambara, S., The influence of dielectric materials on CO_2 conversion performance of pulsed micro-gap cylindrical dielectric barrier discharge reactor, *Jpn. J. Appl. Phys*., Vol. 62, SN1006, 2023.
[23] Khunda, D., Li, S., Cherkasov, N., Rishard M.Z.M., Chaffee, A.L., and Rebrov, E.V., Effect of temperature on the CO_2 splitting rate in a DBD microreactor, *React. Chem. Eng*., Vol. 8, pp. 2223−2233, 2023.
[24] Hosseini Rad, R., Brüser, V., Schiorlin, M., Schäfer, J., and Brandenburg, R., Enhancement of CO_2 splitting in a coaxial dielectric barrier discharge by pressure increase, packed bed and catalyst addition, *Chem. Eng. J.*, Vol. 456, 141072, 2023.
[25] Spencer L. F. and Gallimore A. D., Efficiency of CO_2 dissociation in a radio-frequency discharge, *Plasma Chem. Plasma Process*., Vol. 31, pp. 79–89, 2011.
[26] Berthelot A., and Bogaerts A., Modeling of CO_2 splitting in a microwave plasma: How to improve the conversion and energy efficiency, *J. Phys. Chem. C*, Vol. 121, pp. 8236−8251, 2017.
[27] Yamasaki H., Kamei S., Kuroki T., and Okubo M., Adsorbed CO_2 dissociation using argon and helium nonthermal plasma flows, *IEEE Trans. Ind. Applicat.,* Vol. 56, pp. 6983−6982, 2020.
[28] Wakimoto H., Yamasaki H., Kuroki T., and Okubo M., High-efficiency carbon dioxide reduction using catalytic nonthermal plasma desorption, *Mech. Eng. J*., Vol. 10, 22-00191, 2023.
[29] Wakimoto H., Yamasaki H., Kuroki T., and Okubo M., Performance evaluation of nonthermal plasma carbon dioxide reduction to fuel with dielectric barrier discharge, *J. Electrostat.*, Vol. 130, 103952, 2024.
[30] Lu N., Liu N., Zhang C., Su Y., Shang K., Jiang N., Li J., and Wu Y., CO_2 conversion promoted by potassium intercalated g-C_3N_4 catalyst in DBD plasma system, *Chem. Eng. J*., Vol. 417, 129283, 2021.